iScience

CellPress
OPEN ACCESS

Article

Multimodal assessment of spasticity using a point-of-care instrumented glove to separate neural and biomechanical contributions

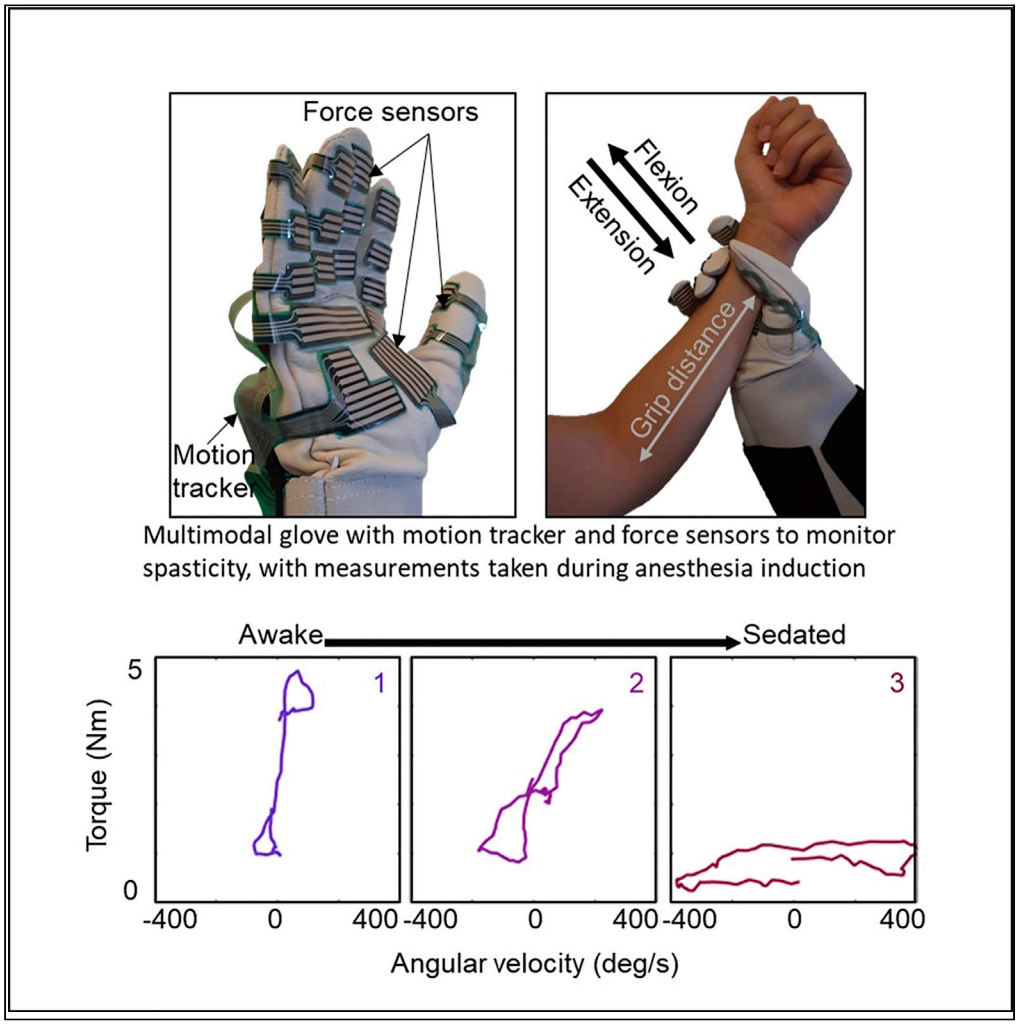

Moran Amit, Cagri Yalcin, Jiaxi Liu, Andrew J. Skalsky, Harinath Garudadri, Tse Nga Ng

tnn046@ucsd.edu

Highlights

Tool to shift from subjective scales to objective metrics in spasticity evaluation

Develop a multifaceted metric to rank severity based on biomechanical properties

Delineate effects of hyper-reflexes and structural abnormalities in spastic muscles

Amit et al., iScience 25, 105286
November 18, 2022
https://doi.org/10.1016/j.isci.2022.105286

iScience

CellPress
OPEN ACCESS

Article

Multimodal assessment of spasticity using a point-of-care instrumented glove to separate neural and biomechanical contributions

Moran Amit,[1] Cagri Yalcin,[2,3] Jiaxi Liu,[1] Andrew J. Skalsky,[4,5] Harinath Garudadri,[2] and Tse Nga Ng[1,6,*]

SUMMARY

Accurate assessment of spasticity is crucial for physicians to select the most suitable treatment for patients. However, the current clinical practice standard is limited by imprecise assessment scales relying on perception. Here, we equipped the clinician with a portable, multimodal sensor glove to shift bedside evaluations from subjective perception to objective measurements. The measurements were correlated with biomechanical properties of muscles and revealed dynamic characteristics of spasticity, including catch symptoms and velocity-dependent resistance. Using the biomechanical data, a radar metric was developed for ranking severity in spastic knees and elbows. The continuous monitoring results during anesthesia induction enable the separation of neural and structural contributions to spasticity in 21 patients. This work delineated effects of reflex excitations from structural abnormalities, to classify underlying causes of spasticity that will inform treatment decisions for evidence-based patient care.

INTRODUCTION

Spasticity is a chronic neuromuscular disorder that is commonly manifested in patients suffering from cerebral palsy, stroke, or traumatic brain injury, etc., affecting over 12 million people worldwide (Barnes et al., 2017; Kuo and Hu, 2018; Crema et al., 2022). Symptoms of spasticity include abnormal muscle stiffness, painful contractures, and jerky movement that impair balance competence and self-care activities (Skalsky and Dalal, 2015; Rekand, 2010; Lance, 1980; Thibaut et al., 2013). Evaluation of the severity level of spasticity is a crucial step in selecting appropriate types of treatment and dosage to prevent progressive deformities and improve quality of life for patients. However, current clinical evaluations are limited by imprecise subjective ratings based on perception, such as the Modified Ashworth Scale and the Tardieu Scale. The subjective ratings are known to be inconsistent and not sensitive (Alhusaini et al., 2010; Fleuren et al., 2010; Puzi et al., 2019; Malhotra et al., 2009) and as such undermines efforts to accurately track and understand the efficacy of different therapies. Clinicians need weeks or months to confirm definite patient deteriorations before escalating treatment to avoid overdosage of medications. Consequently, it has been difficult to manage spasticity, and objective tools that facilitate sensitive, frequent assessments are urgently needed to enable timely interventions and improve patient care.

To address the need for better tools for assessment, previous research had engineered surface electromyography (EMG), ultrasound, and biomechanical measurements to characterize spastic muscles. EMG is meant to capture involuntary muscle activations, but this technique suffers from low signal reproducibility due to issues with electrode placement and motion artifacts (Misgeld et al., 2016; Sloot et al., 2017; Yu et al., 2020; Wang et al., 2017). Ultrasound has been used to inspect muscle fiber lengths and cross-sectional area that relate to muscle strength (Moreau et al., 2009; Cunningham and Loram, 2020). Yet this method does not address the motion-dependent aspects of spasticity. Alternatively, biomechanical measurement tools including myometer and dynamometer were demonstrated to quantify the resistance torque of spastic limbs (Le-Ngoc and Jansse, 2012; Li et al., 2017; Ferreira et al., 2013; Lee et al., 2017; Seth et al., 2015; Wu et al., 2018; Song et al., 2018). Multimodal approaches that combine movement and muscle resistance measurements have been developed to examine the velocity-dependent characteristics of spastic muscles (Wu et al., 2018; Bar-On et al., 2013). However, prior instrumentations are large, motorized structures that are unwieldy to fit onto patients and pose safety risks and adoption barriers for point-of-care settings.

[1]Department of Electrical and Computer Engineering, University of California San Diego, La Jolla, CA 92093, USA

[2]Qualcomm Institute, University of California San Diego, La Jolla, CA 92093, USA

[3]Institute of Medical Engineering, Faculty of Electrical Engineering and Information Technology, Otto-von-Guericke University Magdeburg, Magdeburg, Germany

[4]Department of Orthopedic Surgery, University of California San Diego, La Jolla, CA 92093, USA

[5]Rady Children's Hospital, San Diego, CA 92123, USA

[6]Lead contact

*Correspondence: tnn046@ucsd.edu

https://doi.org/10.1016/j.isci.2022.105286

To overcome this issue with cumbersome equipment, we have developed a multimodal sensor glove for spasticity evaluation (Amit et al., 2019; Yalcin et al., 2020; Jonnalagedda et al., 2016). The device is intended to be worn by caregivers to objectively record the applied torque and movement trajectory while conducting assessment maneuvers on patients. Our portable system offers point-of-care measurements building on recent advances in wearable flexible electronics (Moin et al., 2021; Amit et al., 2019; Zhai et al., 2020; Bonnassieux et al., 2021). Here, we demonstrate the translation of our sensor glove technology to bedside use. With the objective measurements collected using the sensor glove, the severity of spasticity in a patient can be tracked with better accuracy than through the subjective clinical scales based on perception. Furthermore, we envision that with the use of this device, adjustment to medication dosage can be correlated with quantitative data in the future, to improve the assessment of medication efficacy.

The muscle tone in spasticity is comprised of passive, reflexive, and voluntary contributions. The passive component is the stiffness due to structural deformity in the muscle. The reflexive component is the resistance that originates from the hyperactivity of the nervous system. The voluntary component is the contribution of patient's voluntary movement to the total resistance (Van Der Krogt et al., 2015). This work leverages the fact that spasticity symptoms are altered when patients undergo general anesthesia and therefore provide a convenient approach to probe the upper and lower range of spasticity manifested in the same patient. We made measurements on 21 patients before and after sedation and during the transition period from alertness to sedation under general anesthesia. As anesthesia suppressed neural reflex excitation (Fee and Miller, 2004; Jiang et al., 2020), this study facilitated self-consistent comparisons to separate the neural and structural contributions to spasticity, which until now these contributions have been very challenging to differentiate but are very important for identifying the underlying origins of spasticity and symptom management (Fee and Miller, 2004; Smith et al., 2011; Sinkjær and Magnussen, 1994). For example, it has been suggested that spasticity in patients with predominantly hyperactive reflexes was likely to respond well to functional electrical stimulation, whereas other patients responded less well to the same stimulation therapy (Alhusaini, 2013). Knowing the underlying cause of spasticity is essential for predicting whether a treatment would be effective for personalized care.

Furthermore, we related the torque and movement measurements to biomechanical properties of muscles, by fitting the collected data to an equation of motion based on a Hill-type muscle model (Siebert et al., 2021; Meyer et al., 2011). The trends in fit parameters enabled us to pinpoint appropriate metrics for ranking the severity of spasticity. In this article, we present a comparison scale that reveal changes of spastic muscles in quantitative biomechanical parameters, paving a path to shift the diagnostic paradigm from subjective perception to objective measurements for evidence-based patient care.

RESULTS

Our sensor glove in Figure 1A is comprised of an inertial measurement unit (IMU) on the dorsal side and force-sensitive resistors on the palmar side (Amit et al., 2019; Yalcin et al., 2020; Jonnalagedda et al., 2016). Spatial map of the force-sensing elements is presented in Figure S1. We integrated commercially available sensors, and so the system can be readily duplicated for wide deployment. One feature of our integration work is the synchronization of sensors in order to concurrently measure muscle resistance and motion parameters. This multimodal approach enabled acquiring the dynamic characteristics of spastic muscles to understand the motion-dependent muscle resistance. The conversions of sensor signals to torque and motion data are shown in the STAR methods Section.

In terms of form factors, prior measurement schemes strapped sensors on the patient (Le-Ngoc and Jansse, 2012; Li et al., 2017; Ferreira et al., 2013; Lee et al., 2017; Seth et al., 2015; Wu et al., 2018; Song et al., 2018; Bar-On et al., 2013); in contrast, our design puts the equipment on the evaluator instead. Here, the sensor glove can be used to assess both arms and legs as shown in Figures 1B and 1C. Our design is more generalizable than prior biomechanical modules, which were restricted to one extremity type because they were specialized for specific muscles. Prior devices often had issues with poor fit to different patient sizes, a limitation that our design overcomes. During evaluations using our sensor glove, the patient is passive; voluntary motion is not required from the patient, who may be physically incapable to comply with instructions. The clinician wore the sensor glove to perform standardized flexion and extension maneuvers on patients as normally done in perception-based assessments. To augment current clinical practice, the multimodal glove equipped the clinician to simultaneously record the maneuver trajectories and the torque applied to move spastic muscles, providing vital data for further biomechanical analysis.

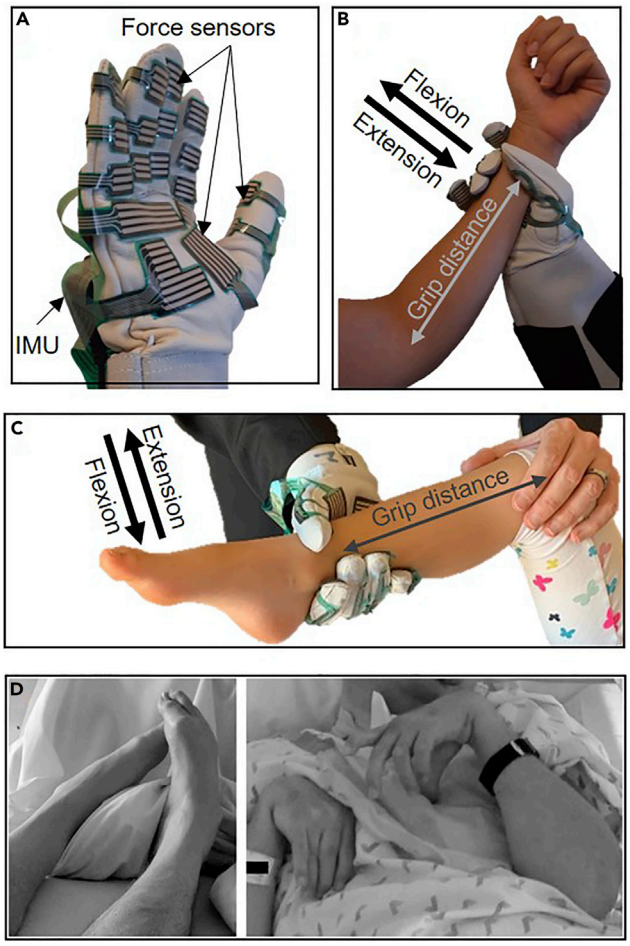

Figure 1. Spasticity measurement

(A) Spasticity assessment glove with IMU and force sensors for simultaneous tracking of motion and torque, respectively. The current design can be used to assess the severity level of spasticity in (B) an arm and (C) a leg.

(D) Photographs of affected limbs due to spasticity (Reproduced with permission from Reference 7. Copyright 2013; Taylor & Francis.).

As a neuromuscular disorder, manifested by abnormal muscle stiffness, painful contractures, and jerky movement (Figure 1D), the abnormal muscle resistance in spasticity can originate from (i) neural impairment: hyperactivity of the nervous system that overly excites muscles and (ii) structural pathology: muscular or connective tissue abnormalities due to denervation, dis-use, or immobilization (Fee and Miller, 2004; Sinkjær and Magnussen, 1994). To better understand this complex combination of acute neural reflexes and chronic effects on structural tissues due to spasticity, we used the sensor glove to track changes in muscle characteristics as patients went under the influence of general anesthesia. The same clinician carried out assessment maneuvers on 21 patients ranging from age 2–26 who received Phenol/Botox nerve block procedure as part of their spasticity treatment. Because anesthesia was necessary for the procedure, the sensor glove measurements were piggybacking on an established process with no additional burden on the patients.

While anesthetics were administered to the patient, the clinician performed flexion and extension maneuvers on the spastic limb continuously until the patient was fully sedated. In Figure 2A, the torque exerted to move the patient's limb was indicative of the resistance of the spastic muscle and steadily decreased as the patient became sedated. For comparison to Figure S2 of the supplemental information, the measurements taken on 3 healthy volunteers with no spasticity show that the applied torque was generally lower in the healthy group due to less muscle resistance than the patients. Simultaneously, the IMU on the sensor glove

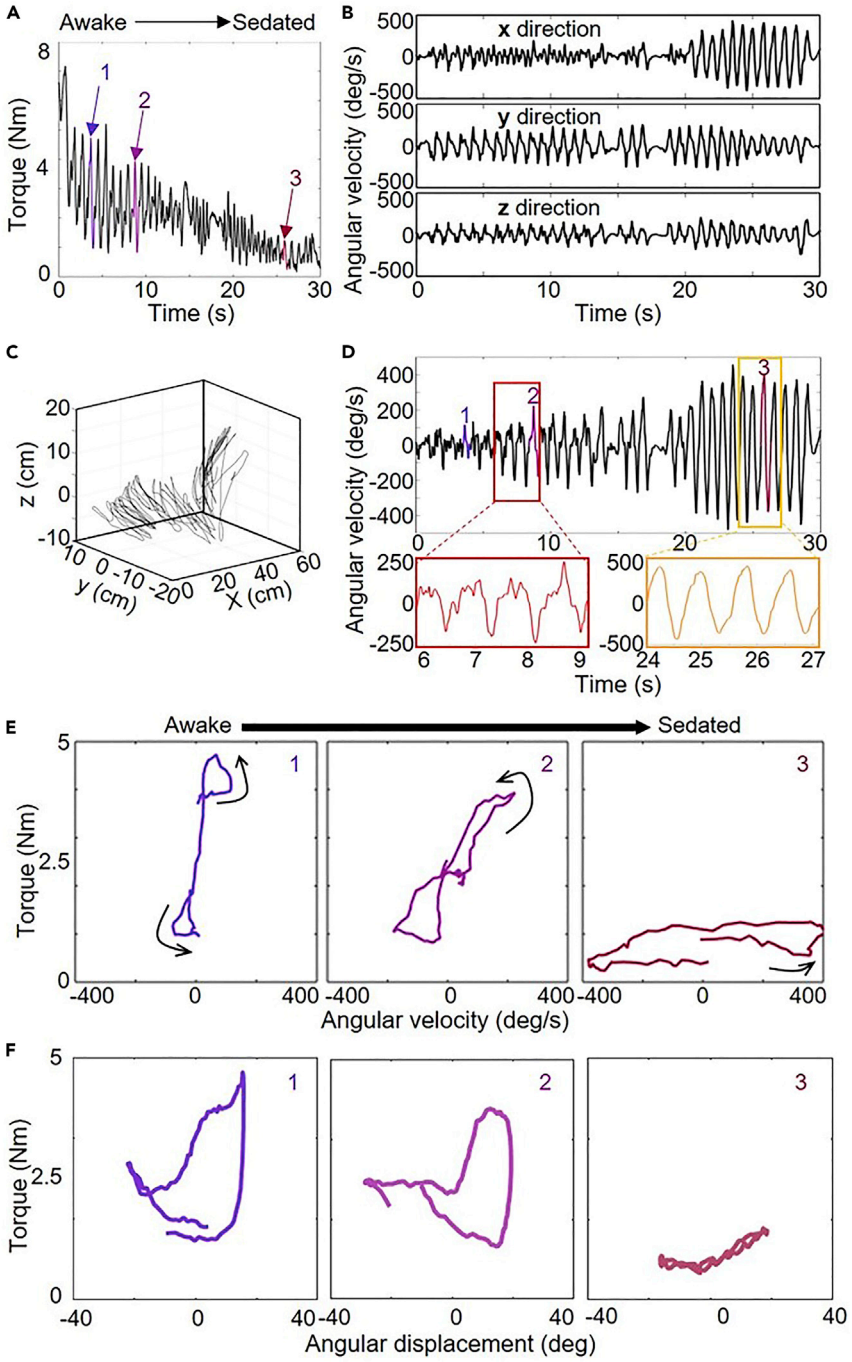

Figure 2. Exemplar measurements on a spastic elbow joint as the patient transitioned from being awake to sedated under general anesthesia

The segments 1, 2, and 3 roughly correspond to awake, partially sedated, and fully sedated conditions.

(A) Torque versus time.

(B) Angular velocity versus time.

(C) Position of the IMU, indicating the trajectory of the IMU throughout the measurement.

(D) Angular velocity along the main axis of movement as determined from principal component analysis on data in part B. Signals taken early in the induction (marked by the red box) were lower in velocity and more abrupt compared to the later stage under full sedation (marked by the orange box).

(E) The evolution of torque versus angular velocity and (F) versus angular displacement as the severity of spasticity decreased. The number labels correspond to the selected maneuver cycles as marked in parts (A and D). The arrows indicate the data flow in the cycle.

recorded the instantaneous maneuver velocity in three-dimensional (3D) space as shown in Figure 2B. The maneuvers were found to be at higher velocities toward the end of the measurement (most prominent in the x-direction), as the patient's muscle resistance decreased in the sedated state. Under anesthesia, we observed suppressed hyperactive reflexes typical of spastic states, suggesting diminished neural mis-firings under sedation. The reverse trend was observed as patients regained consciousness after the anesthesia wore off, in which their muscle resistances significantly increased (Figure S3). In this work, we examined the decrease in the severity of spasticity during anesthesia induction, particularly in aspects of velocity dependence and catch phenomena. Then, the measurement data were correlated with biomechanical parameters, to develop an objective scale for comparing the severity levels of spasticity.

Quantifying the dynamic resistance of spastic muscles

The IMU on the sensor glove captured the maneuver trajectory at the location where the clinician held the patient's limb. The back-and-forth movement cycles of flexion and extension were visualized in 3D space in Figure 2C, where the displacement coordinates were computed from integration of velocities from the 3-axis gyroscope in the IMU. The maneuver trajectory showed a main axis of motion that changes over time. By applying principal component analysis (PCA) transformation, the angular velocity along the axis of maximum motion was obtained in Figure 2D. As the anesthesia took effect on the patient, the velocity signal showed less abrupt changes and was more similar to a sinusoidal waveform, indicating that the maneuver motion was more fluidic and less jerky with the patient under sedation.

After the PCA transformation, the angular velocity along the axis of maximum motion was related to the concurrent torque measurements. We then examined the muscle resistance as a function of movement velocity. The muscle resistance was shown to be different for the flexion and the extension durations, as the muscle groups involved are different. Flexion engages extensor muscles, while extension engages flexor muscles. Note that to change motion directions between flexion and extension, the movement velocity v must reach zero at endpoints of each segment. Hence, we demarcated the segments by $v = 0$ and defined the velocity vector during flexion to be positive and extension to be negative for elbows, and conversely for knees. In our discussions, each maneuver cycle comprises of one flexion segment the consecutive extension segment.

In Figure 2E, we present 3 representative maneuver cycles at the high, medium, and low levels of spasticity as denoted by the number and color labels in Figures 2A and 2D. When the patient was fully awake, the resistance of the spastic muscle was highly dependent on the movement velocity and showed prominent clasp-knife characteristics (Segment 1). Namely, the spastic muscle initially resisted being moved, as manifested in the high torque at the start; but once in motion, the muscle resistance dropped rapidly akin to the sudden closing of a clasp knife. In contrast, when the patient was fully under anesthesia, the measured torque was nearly constant, indicating that the muscle resistance was independent of velocity and not triggered by motion in sedated muscles with suppressed spastic reflex (Segment 3). Thus, in Figure 2E, the evolution of velocity-dependent characteristics of spasticity was precisely captured for the progression from stiff to more fluid movement. In addition, Figure 2F shows the torque as function of the angular displacement. It was observed that when the patient was awake or only partially sedated, torque increased with larger angular displacement. When the patient was fully sedated, the measured torque versus angular displacement was nearly constant with minimal hysteresis.

Figure 3 shows the torque and motion parameters synchronized in time, with the white background designating flexion and gray for extension. As seen from the measurements, it took a longer time to complete a flexion maneuver than an extension, indicating that it was harder to move in the flexion direction and more pronounced spasticity in the extensor muscles. The difference in time to complete flexion and extension maneuvers was reduced when the patient was sedated, as the muscle resistance related to spasticity was lowered. In addition, the maneuvers were more fluid with the patient under sedation, as evident by fewer peaks and less abrupt changes in motion parameters, such as the velocity and its first and second derivatives (acceleration and jerk, respectively) in Figures 3D and 3E. The magnitude of the acceleration and jerk parameters increased because with reduced spasticity the evaluator was able to quickly change the maneuver from flexion to extension.

Another noteworthy measurement result in Figure 3 is the tracking of catch phenomena in spasticity. Catch is described as an abrupt increase in the spastic muscle resistance in response to a fast passive movement

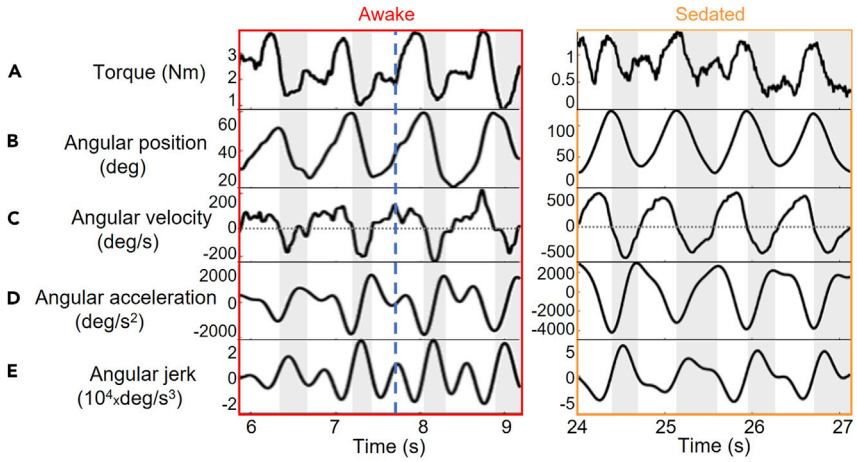

Figure 3. Data captured for flexion and extension

(A) Torque, (B) angular position, (C) angular velocity, (D) angular acceleration, and (E) angular jerk as a function of time for the awake and sedated states, corresponding to Figure 2. Flexion segments are shown with the white background, and extension in gray. The vertical dashed line in blue indicates one of the time points where a catch event occurred. The horizontal dotted line denotes zero velocity and is a guide to determine the endpoints of flexion/extension segments.

before the end of the range of motion (Wu et al., 2018; van den Noort et al., 2010; Lynn et al., 2013). In the awake state, there were peaks in the jerk values accompanied by sharp rises in torque. These jerk peaks with rapid torque increase were indicative of catch events. The dashed blue line in Figure 3 indicates one of the time points when a catch event occurred (the other times when catch was observed were at 6.1 and 6.9 s, but they were not marked by dashed lines to avoid crowding the figure). During a catch phenomenon, there was a sudden decrease in angular velocity, and the angular position showed a plateau, because limb flexion was impeded due to the sudden increase in the muscle resistance.

Demonstrating an objective comparison scale based on biomechanical parameters for ranking the severity of spasticity

The measurements collected during anesthesia induction showed dramatic reductions in spastic symptoms in a short period of 30 s and provided an opportunity to understand how biomechanical attributes would be altered over a wide range of severity levels. We relate the torque and motion measurements to biomechanical properties of muscles, by fitting the data to the following equation of motion:

$$\tau(\theta, t) = I\frac{d^2\theta}{dt^2} + B\frac{d\theta}{dt} + K\theta \qquad \text{(Equation 1)}$$

where τ is the instantaneous torque as a function of angular displacement θ at time t, $d\theta/dt$ is the angular velocity, $d^2\theta/dt^2$ is the angular acceleration, I is the inertial mass, B is the friction coefficient, and K is the spring constant.

The parameters I, B, and K as depicted in Figure 4A are correlated with the Hill's muscle model (Siebert et al., 2021), a mechanical model that represents biomechanical functions using contractile, damper, and elastic elements (more details in Figure S4). The contractile element is ascribed to voluntary force generation through interactions between actin and myosin of the muscles, and it is not used in Equation 1 because in this study the patient muscles were not generating voluntary motion. The damper element accounts for inelastic viscous damping in the soft tissues and is represented by a dashpot with the friction coefficient B. The elastic element models the elasticity of muscles and is represented by a spring with the spring constant K. In addition to the parameters from the Hill's model, we included the term of inertial mass (I) in Equation 1 to account for torque changes due to different limb sizes across patients. The same model is applicable to both spastic elbows and knees.

The above I/B/K model in Equation 1 has been previously used to describe muscle properties (Perreault et al., 2000). Based on the model alone, it cannot separate the neural (reflexive) and non-neural (passive) contributions to muscle resistance, and could only provide an overall evaluation of the biomechanical

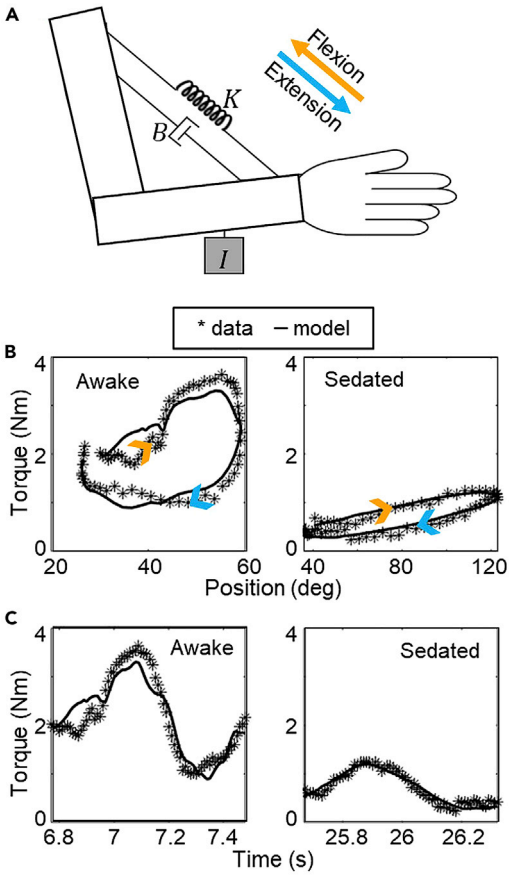

Figure 4. Model fittings

(A) Schematic of the model parameters. Measurement data (asterisk points) and model-fitting results (black solid line) of the applied torque as function of (B) the angular position at the corresponding (C) time, for one maneuver cycle in the awake (left) and sedated (right) states. The arrows represent flexion (yellow) and extension (blue) direction of motion.

properties but not ascribe the mechanisms. However, here we used external conditioning through anesthesia induction to suppress the reflexive/neural component in the patient. In the initial stage when patients were awake, the clinician was moving against the forces contributed by both the non-neural (passive) and the neural (reflexive) components, with the voluntary movement kept minimal. When patients were sedated, the clinician was moving against only the non-neural (passive) forces that were the result of muscle structural deformities.

The biomechanical parameters *I*, *B*, and *K* were extracted for individual maneuver cycles. As mentioned before, each cycle was delineated by the condition of $v = 0$ which denoted the cross-over point when the movement direction was switched between flexion and extension. After the segmentation of data into maneuver cycles, the best-fit values of *I*, *B*, and *K* were computed by fitting Equation 1 to each cycle of flexion and extension measurements. Examples of the fit results are shown in Figures 4B and 4C, which present torque as a function of angular position and time, respectively. The model fitting lines were in excellent agreement with the measurements for this instance, with a correlation coefficient of 93% for the awake state and 96% for the sedated state. The great fit results indicated that Equation 1 is applicable for spastic muscles.

Figure 5 displays trends in nominal measurements and changes in best-fit values of the biomechanical parameters when the severity of spasticity decreased under anesthesia induction. This example shows 29 maneuver cycles during the induction period as presented in Figure 2. The average torque and the torque distribution decreased by 5-fold in Figures 5A and 5B as the patient transitioned from being awake to sedated. For each maneuver cycle, the torque distribution was extracted from the

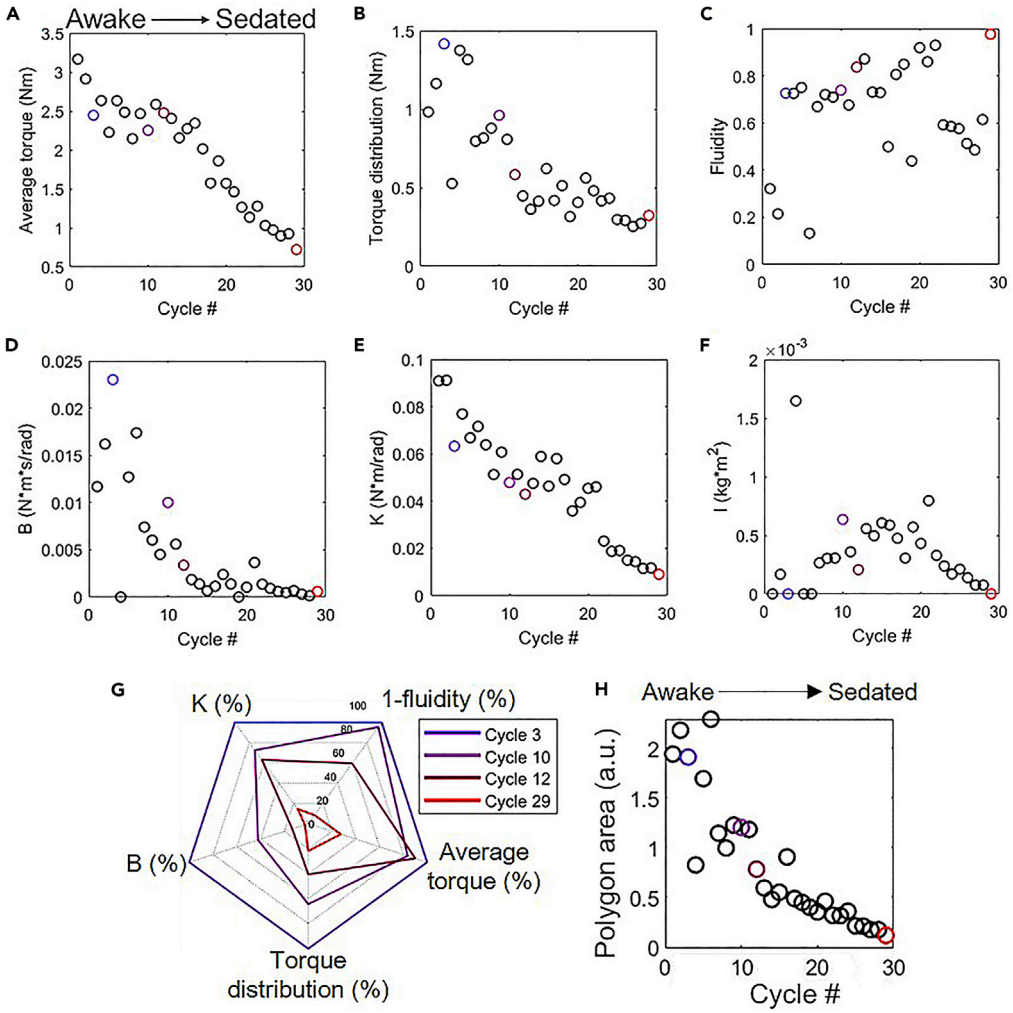

Figure 5. Measurement data and best-fit values of biomechanical parameters in Equation 1, for maneuver cycles on a spastic elbow joint throughout the induction of anesthesia

(A) Average torque, (B) torque variation, (C) movement fluidity, (D) friction coefficient B, (E) spring constant K, and (F) inertial mass I.

(G) Normalized radar plot displaying five parameters that change significantly with the severity level of spasticity. The normalized axes were computed from dividing each parameter by the initial value when spasticity was at its highest (100% = most severe). The color legend denotes the maneuver cycles, as the level of spasticity decreased from severe (cycle #3, purple) to mild (cycle #29, red). The data points used to construct the chart in part G are color coded in parts A to F correspondingly.

(H) Polygon area, defined as the area bounded by the parameter quantities on the radar chart, as a function of the maneuver cycle number.

corresponding histogram of torque values, in which the distribution was the value of one SD from the mean. The movement fluidity was defined to be the correlation coefficient comparing the recorded maneuver velocity to the best-fit sine function of y = a1*sin(b1*x + c1). The fluidity parameter was increasing with later cycles in Figure 5C, as spasticity became less apparent with sedation. The biomechanical quantities of *I*, *B*, and *K* in Equation 1 were varied to fit torque and motion data. The correlation coefficients of fit results are shown for every maneuver cycle in Figure S5. Most of the correlation coefficients were above 50%, and out of 29 fits, there were 7 outliers with correlation coefficient below 50%, in cycle numbers 13–16 and 18–20. The outliers were probably interrupted maneuvers, in which the clinician deviated significantly from the standardized motion. The poor fits with correlation coefficient below 50% were excluded from subsequent analyses.

During the awake to sedated transition, the friction coefficient *B* of the spastic elbow joint dropped by 200-fold in Figure 5D. The spring constant *K* decreased by 10-fold in Figure 5E. These trends reveal the reduction of viscous damping and elastic energy storage in spastic muscles as neural reflexes was suppressed by anesthesia. The large reduction in *B* is also evident in Figure 4B, which presents the torque hysteresis as a function of angular position. The hysteresis indicates an energy loss due to frictional drag. With decreasing hysteresis areas observed during anesthesia induction, it implies less energy dissipation in sedated muscles with lower resistance. Regarding the parameter of inertial mass *I*, the best-fit values in Figure 5F were relatively unchanged between the start and end of data collection. Such fit results are reasonable, since the limb mass is not expected to change in the short measurement duration, while some of the fluctuations in mass values might be due to slight shifts in the inertial center of mass during movement.

Based on the analysis in Figure 5, we identified the five parameters that were substantially altered when the manifestation of spasticity changed under anesthesia. Figure 5G presents those parameters in a radar plot, which offers a summarizing metric to compare the severity levels of spasticity. The axes are normalized to highlight the changes in each parameter. For each maneuver, the data points on radial axes were connected and visualized as a polygon. The polygon area decreased when the severity of spasticity was reduced with sedation, as shown in Figure 5H. Thus, the polygon area can be used as a metric calculation that links the five parameters to rank the severity of spasticity symptoms.

Using the radar plot approach, we analyzed the measurements collected from 22 different spastic limbs and calculated the polygon areas at the highest and lowest level of spasticity for each individual case in Figure 6. The measurements were done on 21 patients, in which an individual was evaluated for both knee and elbow. The polygon area was computed from radial axes with different physical units; as such, the area did not correlate with a single physical unit but was rather a plotting concept in an arbitrary unit. The radar plots used to calculate the polygon areas in Figure 6 are provided in Figure S6. The parameters from 4 cycles in the completely awake or fully sedated state were averaged, and the variations among the 4 cycles were indicated by the error bars of one SD. The data in Figure 6 were categorized according to the inspected joints, which were knees and elbows.

Across the 22 cases here, the polygon area was a practical proxy for the severity level of spasticity and decreased under the effect of anesthesia. The glove sensor data were able to show the change in muscle resistance, whereas the corresponding Modified Ashworth Scale ratings lacked the resolution to provide meaningful interpretation. The numerical values of polygon areas for the knees were generally higher than the elbows, but this difference was mainly due to the higher torque exerted to move heavier knee joints and did not necessarily signify that spasticity was more severe in knees than elbows. Additional data collection will enable us to refine evaluation metrics in the future. One approach is to use the inertial mass parameter to account for weight gain or fluctuations in patients over longitudinal studies. In our current analysis method, we do not focus on cross-patient comparison given the uncertainties in considering different body parts and patient sizes. However, intra-patient comparison of the polygon area values is meaningful and self-consistent.

Considering an individual subject, the relative difference in polygon areas is reliable and reveals the contribution of neural hyperactivities to spasticity in individual patients. In the fully awake state, the patient's spasticity was affected by both neural and structural pathologies; but in the fully sedated state, hyper-reflexes were diminished, thus removing neural contributions to spasticity. In the sedated condition, the remaining muscle resistance was attributed to underlying mechanical structures. Long-term continuous deformities in muscle structures may be caused by the persistent muscle contractions in spasticity as found from biopsies (Smith et al., 2011). In Figure 6, majority of the cases showed large drops in polygon areas, *i.e.*, significant decreases in severity levels when neural reflexes were suppressed by anesthesia. However, in 6 out of the 22 cases (Case #3, 10, 13, 19, 20, and 21), the changes in severity levels between awake and sedated states were $\leq$22%. For these cases, the manifestation of spasticity appeared to be dominated by chronically altered muscles in the affected limbs, and hence, eliminating neural mis-firings did not relieve muscle resistance from abnormal structures.

Here, our measurement procedure to separate neural and structural contributions can offer important clues on sources of spasticity to inform treatment decisions. For example, patients whose spasticity primarily involved hyperactive reflexes may see immediate improvements with medications like Botox that act on

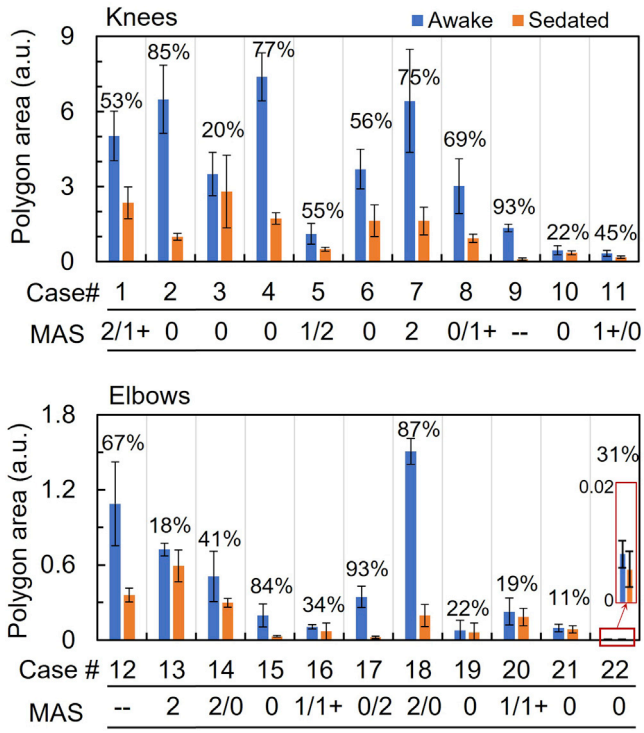

Figure 6. Comparisons of the polygon areas calculated from measurements on spastic knee and elbow joints

Data are represented as +/− one SD. The values were averages of 4 maneuver cycles when patients were awake or fully sedated, correlating to the maximum and minimum level of severity within each case. The percentage denoted for each case represents the change in polygon area from awake to sedated states, with the calculation explained in the STAR method. The Modified Ashworth Scale (MAS) rating taken during the awake state is presented for each case. The MAS ratings under sedation were all 0 for every case. The "2/1+" means the MAS of flexor muscle was 2, while extensor muscle was 1+. A single number such as "2" means the MAS for flexor and extensor were both 2. The '–' means MAS for that patient was not recorded.

the nervous system. For patients who do not show significant difference in severity (polygon areas) between awake and sedated states, their muscle structures have been gradually altered by spasticity over a long term. For them, treatments to relieve and prevent underlying structural problems may be necessary, such as through surgery and physical therapy for restoring functions.

DISCUSSION

This report presents a new quantitative procedure to investigate the biomechanical and neural contributions to spasticity. The multimodal sensor glove in this study offers a convenient, versatile approach to take bedside measurements that objectively monitor dynamic characteristics of spasticity, such as catch symptoms and velocity-dependent resistance. The advantage of our portable system enables continuous monitoring of patients during anesthesia induction. To the best of our knowledge, it is the first point-of-care demonstration that captures large changes in muscle resistance that patients would experience depending on the severity of their neural hyperactivities. These measurements leveraging anesthesia are valuable for classifying underlying causes of spasticity, to delineate effects of reflex excitations and structural abnormalities and inform treatment decisions for different individuals.

The evolution of torque and motion measurements during the sedation period provided a wide coverage of severity levels in spasticity. Those data were well fitted with an equation of motion to identify changes in biomechanical properties of the passive limbs. Biomechanical parameters including friction coefficient and spring constant were shown to closely track the reduction in spasticity. In addition to those two biomechanical parameters, we also used the measured torque, torque variation, and motion fluidity to develop a radar scale connecting the five parameters as a metric to rank the level of severity in spastic knees and elbows.

The metric is built on biomechanical basis and addresses a key problem of inconsistency in the current benchmark scales based on perception.

This work presents opportunities to transform diagnostics and intervention of neuromuscular disorders such as spasticity by augmenting subjective evaluations with objective metrics that can be gathered by trained caregivers in addition to clinicians. With standardized measurements, the portable sensor glove system can potentially facilitate at-home monitoring in the future and provide access to frequent, precise measurements to manage patients' chronic symptoms and improve their quality of life.

Limitations of the study

The limitations of this study include two items. The first is the choice in limiting measurements to patients who needed surgeries that required general anesthesia. This choice afforded us the control to suppress neural activities and consequently distinguish neural and structural contributions to spasticity in the current study. However, for future studies, we should expand the patient pool to those that do not need surgery and hence will not be subjected to anesthesia. The objective sensor glove measurements will be generally useful on all patients for extracting biomechanical properties of their spastic limbs, and the new capability to track those metrics as presented in this work will aid in monitoring treatment efficacies. The second limitation is that this study has not yet examined the consistency in measurements taken by different raters. All measurements here were done by the same clinician (Dr. Skalsky) to reduce uncertainties due to grip variations. We have shown that the glove sensor measurements were reproducible and differed by less than 25% across different trials by the same rater, but with different raters, grip effects may be larger. This should be evaluated in the future and probably be mitigated by implementing neural-network supervised learning (Yalcin et al., 2020), which may also be useful in minimizing the intra-rater variability. Nonetheless, in comparisons between measurements carried out by two different raters on the same patients, the catch characteristics were reproducibly captured as shown in Figure S7 in the Supplemental Information, and this consistent result is promising for future inter-rater studies.

STAR★METHODS

Detailed methods are provided in the online version of this paper and include the following:

- KEY RESOURCES TABLE
- RESOURCE AVAILABILITY
  - Lead contact
  - Materials availability
  - Data and code availability
- EXPERIMENTAL MODEL AND SUBJECT DETAILS
  - Human studies
- METHOD DETAILS
  - Data collection setup and device components
  - Spasticity evaluation procedure
  - Data analysis
- QUANTIFICATION AND STATISTICAL ANALYSIS
  - Software
  - Correlation coefficients in the IBK fits and the fluidity parameter
  - Figure 6. Radar plot percentile change
  - Figure 6. SD and error bar of radar plot area
  - Sample size

SUPPLEMENTAL INFORMATION

Supplemental information can be found online at https://doi.org/10.1016/j.isci.2022.105286.

ACKNOWLEDGMENTS

M.A. and T.N.N. are grateful for the support from the Hartwell Foundation Individual Biomedical Research Award and National Science Foundation CBET#2054517. M.A. was partially supported by the Postdoctoral Fellowship for Women Scientists from the Planning and Budgeting Committee, the Council for Higher Education, Israel.

AUTHOR CONTRIBUTIONS

M.A. and C.Y. developed the instrumented glove system. A.S. collected the patient data. M.A., J.L., and T.N.N. analyzed and interpreted the data. H.G., A.S., and T.N.N. designed the study. M.A. performed the statistical analysis. M.A., J.L., A.S., and T.N.N. have unrestricted access to all data. M.A. prepared the first draft of the manuscript, and all authors contributed to the discussion of results and writing and editing of the manuscript. All authors have read and approved the final draft, agreed to submit the manuscript, and take full responsibility of its content, including the accuracy of the data and the fidelity of the trial to the registered IRB protocol and its statistical analysis.

DECLARATION OF INTERESTS

The authors declare the work here is related to a patent USPTO 20210401372 "Hypertonicity Measuring Device and Method" issued to H.G., A.S., and T.N.N.

Received: January 24, 2022
Revised: September 7, 2022
Accepted: October 4, 2022
Published: November 18, 2022

REFERENCES

Alhusaini, A.A.A., Dean, C.M., Crosbie, J., Shepherd, R.B., and Lewis, J. (2010). Evaluation of spasticity in children with cerebral palsy using Ashworth and Tardieu Scales compared with laboratory measures. J. Child Neurol. *25*, 1242–1247. https://doi.org/10.1177/0883073810362266.

Alhusaini, A.A. (2013). Functional effects of neural impairments and subsequent adaptations. In Cerebral Palsy in Infancy: Targeted Activity to Optimize Early Growth and Development (Roberta Shepherd), pp. 87–106. https://doi.org/10.1016/B978-0-7020-5099-2.00004-2.

Amit, M., Chukoskie, L., Skalsky, A.J., Garudadri, H., and Ng, T.N. (2019). Flexible pressure sensors for objective assessment of motor disorders. Adv. Funct. Mater. 1905241. https://doi.org/10.1002/adfm.201905241.

Amit, M., Mishra, R.K., Hoang, Q., Galan, A.M., Wang, J., and Ng, T.N. (2019). Point-of-use robotic sensors for simultaneous pressure detection and chemical analysis. Mater. Horiz. *6*, 604–611. https://doi.org/10.1039/c8mh01412d.

Barnes, M., Kocer, S., Murie Fernandez, M., Balcaitiene, J., and Fheodoroff, K. (2017). An international survey of patients living with spasticity. Disabil. Rehabil. *39*, 1428–1434. https://doi.org/10.1080/09638288.2016.1198432.

Bar-On, L., Aertbeliën, E., Wambacq, H., Severijns, D., Lambrecht, K., Dan, B., Huenaerts, C., Bruyninckx, H., Janssens, L., Van Gestel, L., et al. (2013). A clinical measurement to quantify spasticity in children with cerebral palsy by integration of multidimensional signals. Gait Posture *38*, 141–147. https://doi.org/10.1016/j.gaitpost.2012.11.003.

Bonnassieux, Y., Brabec, C.J., Cao, Y., Carmichael, T.B., Chabinyc, M.L., Cheng, K.T., Cho, G., Chung, A., Cobb, C.L., Distler, A., et al. (2021). The 2021 flexible and printed electronics roadmap. Flex. Print. Electron. *6*, 023001.

Crema, A., Bassolino, M., Guanziroli, E., Colombo, M., Blanke, O., Serino, A., Micera, S., and Molteni, F. (2022). Neuromuscular electrical stimulation restores upper limb sensory-motor functions and body representations in chronic stroke survivors. Med *3*, 58–74.e10. https://doi.org/10.1016/j.medj.2021.12.001.

Cunningham, R.J., and Loram, I.D. (2020). Estimation of absolute states of human skeletal muscle via standard B-mode ultrasound imaging and deep convolutional neural networks. J. R. Soc. Interface *17*, 20190715. https://doi.org/10.1098/rsif.2019.0715.

Fee, J.W., and Miller, F. (2004). The Leg Drop Pendulum Test performed under general anesthesia in spastic cerebral palsy. Dev. Med. Child Neurol. *46*, 273–281. https://doi.org/10.1111/j.1469-8749.2004.tb00482.x.

Ferreira, J., Moreira, V., Machado, J., and Soares, F. (2013). Improved biomedical device for spasticity quantification. In 2013 IEEE 3rd Portuguese Meeting in Bioengineering (ENBENG) (IEEE), pp. 1–4. https://doi.org/10.1109/ENBENG.2013.6518417.

Fleuren, J.F.M., Voerman, G.E., Erren-Wolters, C.V., Snoek, G.J., Rietman, J.S., Hermens, H.J., and Nene, A.V. (2010). Stop using the Ashworth Scale for the assessment of spasticity. J. Neurol. Neurosurg. Psychiatry *81*, 46–52.

Jiang, W., Zhan, Q., Wang, J., Mei, R., and Xiao, B. (2020). Intraoperative neurophysiological monitoring in selective dorsal rhizotomy (SDR). Brain Sci. Advances *6*, 56–67. https://doi.org/10.26599/bsa.2020.9050009.

Jonnalagedda, P., Deng, F., Douglas, K., Chukoskie, L., Yip, M., Ng, T.N., Nguyen, T., Skalsky, A., and Garudadri, H. (2016). An instrumented glove for improving spasticity assessment. In IEEE Healthcare Innovation Point-of-Care Technologies Conference (IEEE), pp. 167–170. https://doi.org/10.1109/HIC.2016.7797723.

Kuo, C.L., and Hu, G.C. (2018). Post-stroke spasticity: a review of epidemiology, pathophysiology, and treatments. Int. J. Gerontol. *12*, 280–284. https://doi.org/10.1016/j.ijge.2018.05.005.

Lance, J.W. (1980). Pathophysiology of Spasticity and Clinical Experience with Balcofen, Spasticity: Disordered Motor Control, pp. 185–204.

Lee, D.J., Bae, S.J., Jang, S.H., and Chang, P.H. (2017). Design of a clinically relevant upper-limb exoskeleton robot for stroke patients with spasticity. IEEE Int. Conf. Rehabil. Robot. *2017*, 622–627. https://doi.org/10.1109/ICORR.2017.8009317.

Le-Ngoc, L., and Jansse, J. (2012). Validity and reliability of a hand-held dynamometer for dynamic muscle strength assessment. Rehabil. Med. 53–66. https://doi.org/10.5772/37688.

Li, X., Shin, H., Li, S., and Zhou, P. (2017). Assessing muscle spasticity with Myotonometric and passive stretch measurements: validity of the Myotonometer. Sci. Rep. *7*, 44022. https://doi.org/10.1038/srep44022.

Lynn, B.O., Erwin, A., Guy, M., Herman, B., Davide, M., Ellen, J., Anne, C., and Kaat, D. (2013). Comprehensive quantification of the spastic catch in children with cerebral palsy. Res. Dev. Disabil. *34*, 386–396. https://doi.org/10.1016/j.ridd.2012.08.019.

Malhotra, S., Pandyan, A.D., Day, C.R., Jones, P.W., and Hermens, H. (2009). Spasticity, an impairment that is poorly defined and poorly measured. Clin. Rehabil. *23*, 651–658. https://doi.org/10.1177/0269215508101747.

Meyer, G.A., McCulloch, A.D., and Lieber, R.L. (2011). A nonlinear model of passive muscle viscosity. J. Biomech. Eng. *133*, 091007. https://doi.org/10.1115/1.4004993.

Misgeld, B.J.E., Luken, M., Heitzmann, D., Wolf, S.I., and Leonhardt, S. (2016). Body-sensor-network-based spasticity detection. IEEE J. Biomed. Health Inform. *20*, 748–755. https://doi.org/10.1109/JBHI.2015.2477245.

Moin, A., Zhou, A., Rahimi, A., Menon, A., Benatti, S., Alexandrov, G., Tamakloe, S., Ting, J., Yamamoto, N., Khan, Y., et al. (2021). A wearable biosensing system with in-sensor adaptive machine learning for hand gesture recognition. Nat. Electron. *4*, 54–63. https://doi.org/10.1038/s41928-020-00510-8.

Moreau, N.G., Teefey, S.A., and Damiano, D.L. (2009). In vivo muscle architecture and size of the rectus femoris and vastus lateralis in children and adolescents with cerebral palsy. Dev. Med. Child Neurol. *51*, 800–806. https://doi.org/10.1111/j.1469-8749.2009.03307.x.

Perreault, E.J., Crago, P.E., and Kirsch, R.F. (2000). Estimation of intrinsic and reflex contributions to muscle dynamics: a modeling study. IEEE Trans. Biomed. Eng. *47*, 1413–1421. https://doi.org/10.1109/TBME.2000.880092.

Puzi, A.A., Sidek, S.N., Khairuddin, I.M., Md Yusof, H., and Mat Rosly, H. (2019). Inter-rater and intra-rater reliability of quantitative upper limb spasticity evaluation based on modified ashworth scale tool. In 2018 IEEE EMBS Conference on Biomedical Engineering and Sciences, IECBES 2018 - Proceedings, pp. 126–130. https://doi.org/10.1109/IECBES.2018.8626688.

Rekand, T. (2010). Clinical assessment and management of spasticity: a review. Acta Neurol. Scand. *122*, 62–66. https://doi.org/10.1111/j.1600-0404.2010.01378.x.

Seth, N., Johnson, D., Taylor, G.W., Allen, O.B., and Abdullah, H.A. (2015). Robotic pilot study for analysing spasticity: clinical data versus healthy controls. J. NeuroEng. Rehabil. *12*, 109. https://doi.org/10.1186/s12984-015-0103-8.

Siebert, T., Screen, H.R.C., and Rode, C. (2021). Computational Modelling of Muscle, Tendon, and Ligaments Biomechanics, 2nd ed. (Elsevier Ltd.). https://doi.org/10.1016/b978-0-12-819531-4.00008-0.

Sinkjær, T., and Magnussen, I. (1994). Passive, intrinsic and reflex-mediated stiffness in the ankle extensors of hemiparetic patients. Brain *117*, 355–363. https://doi.org/10.1093/brain/117.2.355.

Skalsky, A.J., and Dalal, P.B. (2015). Common complications of pediatric neuromuscular disorders. Phys. Med. Rehabil. Clin. N. Am. *26*, 21–28. https://doi.org/10.1016/j.pmr.2014.09.009.

Sloot, L.H., Bar-On, L., van der Krogt, M.M., Aertbeliën, E., Buizer, A.I., Desloovere, K., and Harlaar, J. (2017). Motorized versus manual instrumented spasticity assessment in children with cerebral palsy. Dev. Med. Child Neurol. *59*, 145–151. https://doi.org/10.1111/dmcn.13194.

Smith, L.R., Lee, K.S., Ward, S.R., Chambers, H.G., and Lieber, R.L. (2011). Hamstring contractures in children with spastic cerebral palsy result from a stiffer extracellular matrix and increased in vivo sarcomere length. J. Physiol. *589*, 2625–2639. https://doi.org/10.1113/jphysiol.2010.203364.

Song, S.Y., Pei, Y., Tippett, S.R., Lamichhane, D., Zallek, C.M., and Hsiao-Wecksler, E.T. (2018). Validation of a wearable position, velocity, and resistance meter for assessing spasticity and rigidity. In Frontiers in Biomedical Devices - 2018 Design of Medical Devices Conference, pp. 6–9. https://doi.org/10.1115/DMD2018-6906.

Thibaut, A., Chatelle, C., Ziegler, E., Bruno, M.-A., Laureys, S., and Gosseries, O. (2013). Spasticity after stroke: physiology, assessment and treatment. Brain Inj. *27*, 1093–1105. https://doi.org/10.3109/02699052.2013.804202.

van den Noort, J.C., Scholtes, V.A., Becher, J.G., and Harlaar, J. (2010). Evaluation of the catch in spasticity assessment in children with cerebral palsy. Arch. Phys. Med. Rehabil. *91*, 615–623. https://doi.org/10.1016/j.apmr.2009.12.022.

Van Der Krogt, H., Klomp, A., De Groot, J.H., De Vlugt, E., van der Helm, F.C., Meskers, C.G., and Arendzen, J.H. (2015). Comprehensive neuromechanical assessment in stroke patients: reliability and responsiveness of a protocol to measure neural and non-neural wrist properties. J. NeuroEng. Rehabil. *12*, 28. https://doi.org/10.1186/s12984-015-0021-9.

Wang, K., Parekh, U., Pailla, T., Garudadri, H., Gilja, V., and Ng, T.N. (2017). Stretchable dry electrodes with concentric ring geometry for enhancing spatial resolution in electrophysiology. Adv. Healthc. Mater. *6*, 1700552. https://doi.org/10.1002/adhm.201700552.

Wu, Y.N., Park, H.S., Chen, J.J., Ren, Y., Roth, E.J., and Zhang, L.Q. (2018). Position as well as velocity dependence of spasticity- four-dimensional characterizations of catch angle. Front. Neurol. *9*, 863.

Yalcin, C., Sam, M., Bu, Y., Amit, M., Skalsky, A., Yip, M., Ng, T.N., and Garudadri, H. (2020). Artifacts mitigation in sensors for spasticity assessment. Adv. Intell. Syst. 2000106.

Yu, S., Chen, Y., Cai, Q., Ma, K., Zheng, H., and Xie, L. (2020). A novel quantitative spasticity evaluation method based on surface electromyogram signals and adaptive neuro fuzzy inference system. Front. Neurosci. *14*, 462. https://doi.org/10.3389/fnins.2020.00462.

Zhai, Y., Wang, Z., Kwon, K.S., Cai, S., Lipomi, D., and Ng, T.N. (2020). Printing multi-material organic haptic actuators. Adv. Mater. 2002541.

STAR★METHODS

KEY RESOURCES TABLE

REAGENT or RESOURCE	SOURCE	IDENTIFIER
Deposited data		
Patient data	this paper	Mendeley Data Reserved https://doi.org/10.17632/2xg8y52skn.1
Software and algorithms		
MATLAB	MathWorks	https://www.mathworks.com/products/matlab.html
Scripts for analyses	this paper	Mendeley Data Reserved https://doi.org/10.17632/2xg8y52skn.1

RESOURCE AVAILABILITY

Lead contact

Further information and requests for resources and reagents should be directed to and will be fulfilled by the lead contact, Tse Nga Ng (tnn046@eng.ucsd.edu).

Materials availability

This study did not generate new unique reagents.

Data and code availability

- Data

Experimental data have been deposited at Mendeley data https://doi.org/10.17632/2xg8y52skn.1 and are publicly available as of the date of publication. Accession numbers are listed in the key resources table, and the weblink is https://data.mendeley.com/datasets/2xg8y52skn.

- Code

All original code has been deposited at Mendeley data and is publicly available as of the date of publication. DOIs are listed in the key resources table.

- Additional Information

Any additional information required to reanalyze the data reported in this paper is available from the lead contact upon request.

EXPERIMENTAL MODEL AND SUBJECT DETAILS

Human studies

There were 21 human subjects in this study in total. The subject group was mixed gendered, with the age range of 2–26 years old. All patients are cerebral palsy cases. The information regarding the limb diameters and limb length (labeled as 'grip') can be found in the shared data file on Mendeley https://doi.org/10.17632/2xg8y52skn.1. All measurements were taken with written informed consent of the patients and their legal guardians and approved by UCSD Institutional Review Board #180115.

METHOD DETAILS

Data collection setup and device components

To collect and record the data from patient, the instrumented glove was connected to a laptop. The pressure sensors (Tekscan 4256E) on the glove were connected to an analog-to-digital converter (ADC) which passed the data to a hub and from there to a host computer. The host computer ran a LabVIEW executable graphical user interface to capture the data and generate a CSV file for each data collection trial.

The multimodal instrumented glove incorporated resistive force sensors (Tekscan, 4256E) and an IMU (MotionNode). To obtain the applied torque from the sensor glove, the signals from all the force-sensing elements were added together. The summed signals were calibrated against standard weights to convert into corresponding force values. Then to determine torque, the force value was multiplied by the grip distance, defined as the distance between the joint and the center of the glove, as shown in Figures 1B and 1C. In our torque calculations, we assumed a 90° angle between the applied force vector and the limb being evaluated (Figure S1). The angular velocity signals from the 3-axis gyroscope in the IMU were integrated to extract movement trajectories in 3D space. Principal component analysis was implemented for the angular velocity signals to determine the main axis of movement. Specifically, the pca function in MATLAB was used. The angular velocity along the main axis of movement was integrated to obtain the angular position. The same data were differentiated with respect to time, in which the first derivative was calculated to find the angular acceleration, and the second derivative to find the angular jerk.

Spasticity evaluation procedure

The study included 21 cerebral palsy pediatric patients in the age range of 2–26 years old. All spasticity patients in this study underwent a surgical procedure that required general anesthesia. Per each individual patient, the perception-based Modified Ashworth Scale rating was recorded along with the glove measurements. A clinician performed the maneuver measurements with the sensor glove while anesthesia was administered to the patients, to assess their spastic limbs throughout the anesthesia induction procedure. The procedure of measuring from awake to sedated was much faster than our early trials, in which the patients were monitored when they were waking up from anesthesia. Here the experimental time frame was in minutes, while waiting for patients to wake up fully from sedation took at least an hour. We measured the full transition without skipping any state in between awake and fully sedated states, whereas the reverse order (sedated to awake) did not afford this opportunity as it would be very intrusive to continuously maneuver the patient for an extended time.

Data analysis

All patient information and data were stored in a MATLAB structure array. A sample code that was used to analyze patient data has been uploaded in Mendeley Data https://doi.org/10.17632/2xg8y52skn.1, and a read-me file describing how to replicate all plots in this manuscript.

QUANTIFICATION AND STATISTICAL ANALYSIS

Software

MATLAB (MathWorks) and Excel (Microsoft) were used in this work.

Correlation coefficients in the IBK fits and the fluidity parameter

After the best-fit values of I, B, and K were computed by fitting Equation 1 to each cycle of flexion and extension measurements, the I, B, and K were plugged back into Equation 1 to get a simulated torque function. Then the MATLAB function *corrcoef* was used to calculate the correlation coefficient between the recorded torque and the simulated torque. More details of the MATLAB *corrcoef* function can be found at https://www.mathworks.com/help/matlab/ref/corrcoef.html.

The movement fluidity was defined to be the correlation coefficient comparing the recorded maneuver velocity to the best fit sine function of y = a1*sin(b1*x + c1), using fittype('sin1') MATLAB function.

Figure 6. Radar plot percentile change

The polygon area was calculated with the radar plots as shown in Figure S6. The polygon area's percentage change was denoted for each trial on the bar chart. The percentage change was calculated as $\frac{(\text{awake area} - \text{sedated area})}{\text{awake area}} \times 100\%$.

Figure 6. SD and error bar of radar plot area

For each patient's each limb, the radar plot area was the average of 4 maneuver cycles when patients were awake or fully sedated (area used = the sum of all 4 maneuver cycles/4). The SD was calculated with the same 4 maneuver cycles, and the size of sample was 4. The error bar shown in Figure 6 was set to be one SD.

Sample size

There were 21 individual subjects. The reported data included 22 different spastic limbs of the 21 subjects, in which one individual was evaluated for both knee and elbow.